European Rotorcraft Forum

NUMERICAL INVESTIGATION OF QUAD ROTORS IN GROUND EFFECT

Yasutada Tanabe, tan@chofu.jaxa.jp, Japan Aerospace Exploration Agency (JAXA) (JAPAN)
Hideaki Sugawara, sugawara.hideaki@jaxa.jp, JAXA (JAPAN)
Shigeru Sunada, shigeru.sunada@mae.nagoya-u.ac.jp, Nagoya University (JAPAN)
Koichi Yonezawa, koichi-y@criepi.denken.or.jp, Central Research Institute of Electrical Power Industry (CRIEPI) (JAPAN)
Hiroshi Tokutake, tokutake@se.kanazawa-u.ac.jp, Kanazawa University (JAPAN)

Abstract
Flowfield and performance of quad rotors hovering in ground effect (IGE) are investigated through numerical simulations. A variable pitch-controlled quadrotor drone developed for applications in severe gusty circumstances is modeled in the simulations. Compared with a single rotor, the flowfields around the quad rotors are highly complex. The change of rotor performance with the height from the ground is noticeably different comparing to the single rotor case. The required power for a constant thrust does not monotonically decrease with the rotor height, which adds difficulties to the stable flight control near the ground. Comparisons to the quadrotor drone with a central fuselage are also performed. Remarkable differences in the flowfield and rotor performance are found.

1. INTRODUCTION

With the widely spreading developments and applications of drones and eVTOL aircraft, aerodynamic features of multiple rotors increasingly accumulate interests. While the number of rotors on one aircraft can vary from 4 to as many as 32 or even more, the placement of the rotors can also have a vast number of variations. The rotors are interacting aerodynamically with each other and with the surrounding objects, resulting in very complex flowfields around the rotors. Even the flowfields around relatively simple combinations of multiple rotors are not well understood so far.

Quadrotor is the simplest configuration of the drones. Each rotor can be optimized to hovering performance or to forward flight condition individually. However, on a quadrotor drone, the rotor performance is significantly influenced by the gap between the rotors, not to mention the partial or full overlapping rotor layout. Generally, the neighbouring rotors are rotating in different directions, which adds another factor of complexity. When the rotor is in ground effect (IGE), the interaction between the rotor and the ground plane becomes dominant.

As reported by Kohno et al. in Ref. [1], where quad rotors IGE were studied, the distance between the rotors significantly influenced the trend of the ground effect. When the rotor gap is minimal, the overall thrust increases monotonically as the rotor height decreases, resembling the ground effect of a single rotor. When the rotor gap is greater than 0.3 times the rotor radius, the overall thrust gradually decreases as the rotor height decreases. At a rotor height less than the rotor radius, the overall thrust increases abruptly. This trend deviates significantly from that of a single rotor. It is observed that there is flow recirculation as result of the interaction between the rotors and the ground plane, which causes the loss of the rotor thrust at the intermediate rotor height. [2] However, in their studies, the fuselage at the centre of the quadrotors was not considered. The rotors were fixed-pitch propellers. When the rotor height changed, the rotor thrust changed as result of the ground effect, such that the balance between the aircraft gravitational force and the rotor thrust cannot be satisfied.

More realistic simulations in which a constant thrust is generated by trimming the rotor pitch angle for a variable-pitch-controlled quadrotor drone have been conducted by the authors. [3] It is found that the central fuselage may play an important role of a quadrotor type drone IGE. To identify the influence of the central fuselage, in this paper, a set of variable-pitch-controlled quad rotors without the central fuselage is studied. The results are also compared to the single rotor IGE.

2. QUADROTOR DRONE MODELLING

A prototype of variable-pitch-controlled drone of 7 kg in gross weight as shown in Fig. 1 was developed by the authors. [4] It is being utilized for bridge inspections where strong gusts are often encountered. The control of the drone through the rotor-blade pitch-angle variation provides a fast response to the command within a 1/10 of time lag

Presented at 47th European Rotorcraft Forum, United Kingdom, 7-9th September, 2021.

comparing with the general rotor-speed-controlled ones. [5] For the hovering flight near the ground, the rotor rotating speed is kept the same and the rotor pitch angle is changed to generate the same target rotor thrust, same as the case of a single rotor conventional helicopter.

This drone including the central fuselage was studied about its behaviour IGE. [3] When the rotor height was about one rotor radius, flow recirculation around the rotors was observed which caused a loss of rotor performance and might induce instability of flight at this low altitude. The upwash formed in the centre of the drone was blocked by the central fuselage and the flow direction was altered. To understand the aerodynamic influence of the central fuselage, in this paper, quad rotors without the central fuselage IGE are numerically simulated. The results are compared with the quadrotor drone with the central fuselage and also with the single rotor IGE.

Figure 1. A quadrotor drone with variable pitch controls [4]

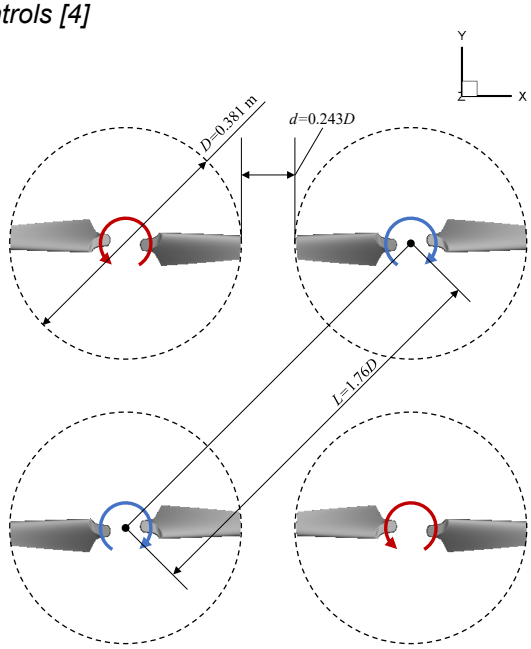

Figure 2. Layout of the quad rotors

The layout of the quad rotors without the central fuselage is illustrated in Fig. 2. The rotor diameter, D, is 0.381 m. The distance between diagonal rotor centres, L, is 1.76D. The rotor gap d is 0.243D. The design parameters of the drone are listed in Table 1. A cambered thin airfoil (OA117) was chosen, and the rotor blade had a linear twist of −21°. The support arms, landing skids, and other details were omitted. Only the rotor blades are considered. The rotor rotating speed is 5400 rpm. The design gross weight of this drone is 7 kg so that each rotor generates an average thrust of 17.15 N during hovering flight.

Table 1. Variable-Pitch Drone design parameters

Number of rotors, N_R	4
Number of blades, N_b	2
Rotor rotational speed	5400 RPM
Rotor radius, R	0.1905 m
Blade root chord, c_r	0.0665 m
Blade tip chord, c_t	0.0402 m
Blade airfoil	OAF117
Blade twist, θ_t	−21° (linear)

3. NUMERICAL METHODOLOGIES

3.1. Numerical methods in rFlow3D

Numerical simulations of the quad rotors IGE are conducted using a rotorcraft CFD code, rFlow3D, an in-house code developed at JAXA. [6]. In the rFlow3D code, a three-dimensional moving overlapping grid method is used. The blade grids move and deform within the inner Cartesian background grid. Generally, a wider outer background Cartesian grid is used to preserve the uniform inflow condition.

A numerical solution is obtained via an interpolation from the inner grids to the outer grid. The update of the flow solution is obtained based on the boundary conditions interpolated from the outer background grid. Any number of rotors can be handled using this code. rFlow3D successfully captured the interactions of a hexa-rotor drone hovering near a side wall or an upper wall. [7] Further details of the computational methods applied to multiple rotors can be found in Ref. [8].

An all-speed numerical scheme, namely, simple low dissipation AUSM (SLAU) [9] with extension to three dimensional moving grids (referred to as mSLAU) [10], is adopted. It is suitable for flow calculation around a rotary wing, where the local flow speed may vary from very low on the blade root area to transonic at the tip. Combining mSLAU with a fourth-order compact MUSCL TVD (FCMT) interpolation scheme [11], fourth-order spatial accuracy can be obtained in shock-free regions. The implicit LU-SGS and dual-time-stepping methods [12] are used for time

integration on blade grids. However, for the background grids, an explicit four-stage Runge-Kutta time integration method [13] is used. In this study, no turbulence model was adopted considering the relatively low Reynolds numbers on the rotors. The numerical methodologies applied to each type of grid are summarized in Table 2.

Table 2. Numerical methodologies

Items	Cartesian background grid	Body-fitted grid (Blade / Fuselage)
Governing equations	Three-dimensional compressible Navier–Stokes equations	
Spatial discretization	Cell-vertex FVM	Cell-centered FVM
Time integration	Four-stage Runge–Kutta method	Dual-time stepping / LU-SGS
Numerical flux	mSLAU (Modified SLAU)	
Reconstruction	FCMT (Fourth-order Compact MUSCL TVD)	
Viscous flux	Second-order central difference method	
Turbulence model	Not applied (QDNS, Quasi-DNS)	

The forces and moments generated by a single rotor are nondimensionalized, as expressed in Eqs. (1) – (4), where C_T is the thrust coefficient, C_Q is the torque coefficient, and C_P is the power coefficient. The figure of merit (*FM*) of a rotor is defined as the ratio of the ideal induced power to the actual required power; the closer it is to 1, the better is the rotor performance in hover.

$$C_T = \frac{T}{\left(\rho\pi R^2 V_{tip}^2\right)} \tag{1}$$

$$C_Q = \frac{Q}{\left(\rho\pi R^2 V_{tip}^2 R\right)} \tag{2}$$

$$C_P = \frac{P}{\left(\rho\pi R^2 V_{tip}^3\right)} = C_Q \tag{3}$$

$$FM(\text{Figure of Merit}) = \frac{(C_T)^{\frac{3}{2}}/\sqrt{2}}{C_P} \tag{4}$$

3.2. Overset computational grid system

The computational overset grid system used in this study is shown in Fig. 3. Only one background Cartesian grid is used. Wall non-slip boundary condition is applied to the background bottom surface to simulate the ground plane. The grid geometry for the blade (8 in total) is shown in Fig. 4. The resolution in the background grid around the rotors was set to 15% of the length of the blade tip chord. Dense grids were placed near the walls to resolve the boundary layer flows on the blade surface and on the ground, as presented in Table 3. In the simulations, rotor height is changed by placing the background grid with vertical translational displacement, so that for all the ground effect simulation cases, the same grid data is used.

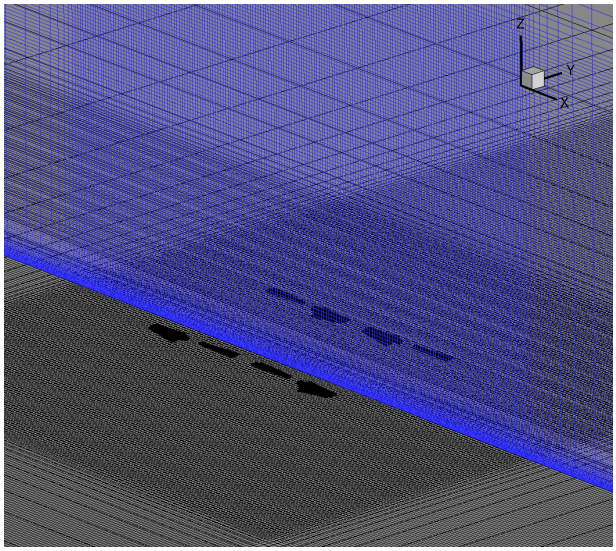

Figure 3. Overset grid system for quad rotors

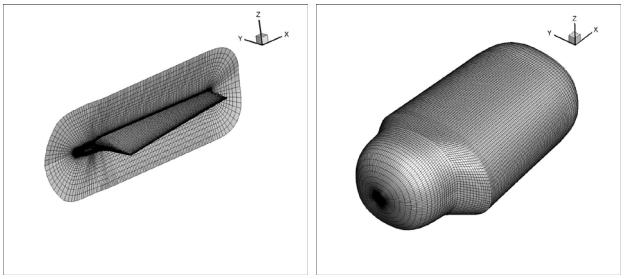

Figure 4. Blade grid

Table 3. Grid points and 1st cell height

Grid	Number of grid points	Height of 1st cell from the wall [m]
Background grid	449 × 449 × 333 (X × Y × Z)	1.0×10^{-3}
Blade grid × 8	121 × 143 × 61 (Span × Chord × Normal)	2.0×10^{-6}
Fuselage grid	*71 × 101 × 45 (Longitudinal × Circumference × Normal)*	*2.0×10^{-5}*

3.3. Rotor test cases

Considering the ground effect generally appears below 1 rotor diameter for a single rotor, and the equivalent rotor area of the quad rotors is same with a single rotor with 2 times of the diameter, the rotor heights selected in this study is listed in Table 4. The rotor height from the ground is varied from 0.25D to

3D. As a reference, the case without a ground plane (out of ground effect, OGE) is also simulated. Small changes of rotor heights between h/D=0.25 to 0.75 are carried out, aiming to capture the phenomena of rotor flow recirculation accompanying with the degradation of rotor performance.

Table 4. Quad rotor test cases

Rotor thrust, *T*, per 1 rotor	17.15 N ($C_T = 0.0106$)
Control	Collective pitch, θ_0
Distance of rotor to ground	*h*/*D* = 0.25, 0.30, 0.35, 0.40, 0.45, 0.50, 0.55, 0.60, 0.65, 0.70, 0.75, 1.0, 2.0, 3.0, OGE

4. RESULTS AND DISCUSSIONS

4.1. Validation of single rotor in ground effect

Before the simulations of the quad rotors, the single rotor in ground effect was studied and validated with the experimental data. The results have been reported in Ref. [5], but the outwash from the rotor on the ground was not developed enough especially for the far locations from the rotor. The computations have been extended.

The single rotor performance OGE has been validated with experiment by the authors before. [14] The rotor power ratio between IGE and OGE for a single rotor is shown in Fig. 5. It is compared with the empirical relationship proposed by Schmas et al. [15]. Excellent agreement is found.

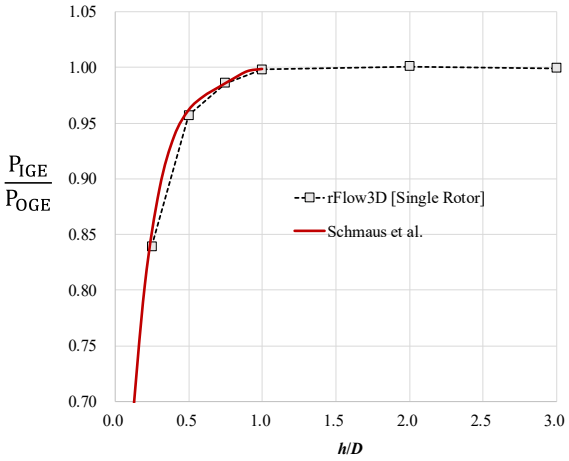

Figure 5. Single rotor power ratio changes with rotor height [5]

An instantaneous flowfield for a single rotor at a rotor height of 0.5 diameters indicated by the vertical velocity component, *w,* normalized by sonic speed, in the rotor central cross section at rotor revolutions of 30 after simulation starts is shown in Fig. 6. Highly unsteady flow along the ground is observed.

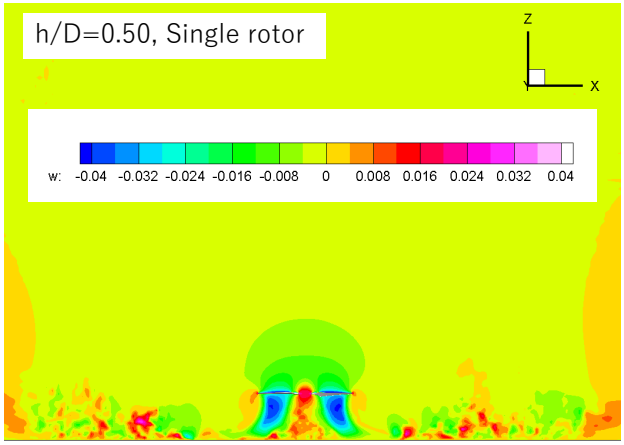

Figure 6. Instantaneous flowfield of a single rotor IGE

To obtain an averaged outwash velocity profile from the computational results, the flow velocity components in the background grid are averaged over 4 rotor revolutions (58-61) every 150 degrees of azimuth angles. Averaged flow velocity normalized by the rotor induced velocity ($v_i = \sqrt{T/2\rho A}$, ρ: air density; A: rotor disc area) is shown in Fig. 7. The influence of the starting vortex still can be noticed beyond the y/D=2.1 station. Further longer computation to obtain a well converged quasi-steady flowfield on the ground may be required. For this study, the outwash profiles at y/D=0.625, 1.0, 1.5, 2.1 are compared with existing measurements.

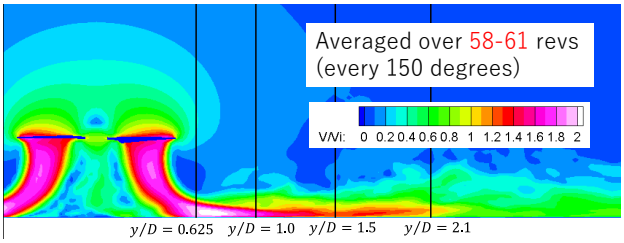

Figure 7. Averaged flowfield of the single rotor IGE

Comparisons of the predicted average outwash profiles, labelled as rFlow3D, with measurements are shown in Fig. 8. The measurement data from NASA [16] was carried out using a real helicopter H-13 in 1961. The measurement data from NDA (National Defence Academy Japan) [17] was carried out using a small scall model rotor in a laboratory. Although the rotor blade geometries and operating conditions are quite different for the three rotors, the outwash profile on the ground looks very similar when the velocity is normalized by the rotor induced velocity and the station divided by the rotor diameter, D, respectively. Please notice that at y/D=1.5 for rFlow3D prediction and NDA, the data from NASA were measured at y/D=1.3. A more general rotor outwash model was proposed by Tanabe et al [18] based on a jet blowing model. For stations far from the rotor, that model can

provide estimations of the maximum velocity and the profile at any station. Near the rotor, direct numerical simulations such as this study can provide detailed information about the unsteady flow structures and improve the understanding of the complex flowfields around the rotor.

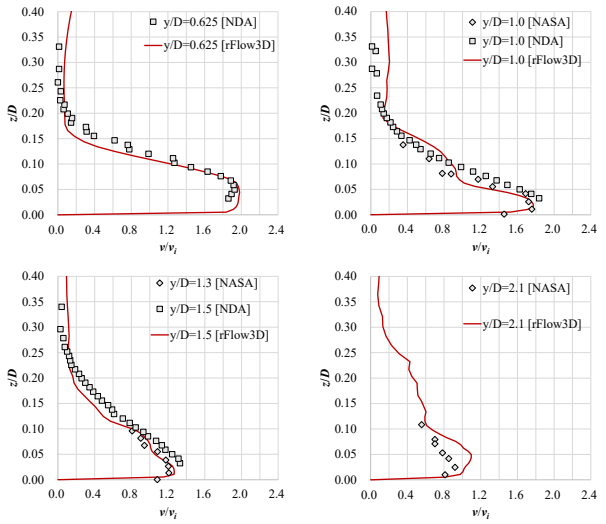

Figure 8. Outwash velocity profiles for a single rotor IGE

4.2. Computational convergence

The flowfield around the quad rotors is very complex and the interaction with the ground plane adds the complexity furthermore. The unsteadiness in the flowfield for a single rotor IGE is already remarkable. For the quad rotors, each rotor may be in a different state of flow variations. In this study, each rotor is trimmed separately to generate the same target thrust. During the computations, the pitch angle of each rotor is adjusted every 1 rotor revolution.

The attained averaged thrust coefficient of the quad rotors after 60 revolutions from simulation starts is shown in Fig. 9. At the rotor heights less than 1.0*D*, smooth thrust convergence becomes difficult. For this study, averaged thrust is within 1% of the target thrust. However, as can be seen in Fig. 10, some rotors have more deviations (about 2%) from the target thrust of each rotor. It seems at rotor height about 0.4*D,* the variations between the rotors are the highest. Also as shown in Fig. 11, the differences of pitch angles between the rotors are large when the rotor height is around 0.5*D*. The flowfield around each rotor is considered quite different at these rotor heights.

The flowfields around the rotors represented by iso-surfaces of the Q-criterion for rotor heights of 0.4*D* and 3.0*D* are shown in Fig. 12. At low rotor heights, upwash in the central portion of the quad rotors is very strong. The upwash directly interacts with the rotors, which is conceivable to be the source of the rotor thrust fluctuations. As can be observed in Fig. 13, the fluctuations of the thrust for the 0.4*D* is much higher than that of the 3.0*D* rotor height.

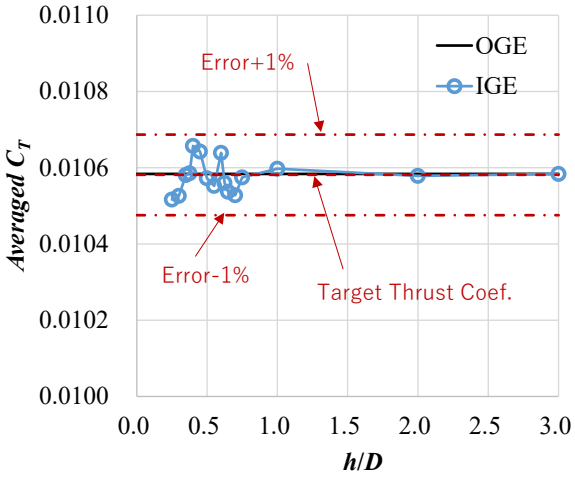

Figure 9. Averaged thrust coefficient of the quad rotors after 60 revolutions

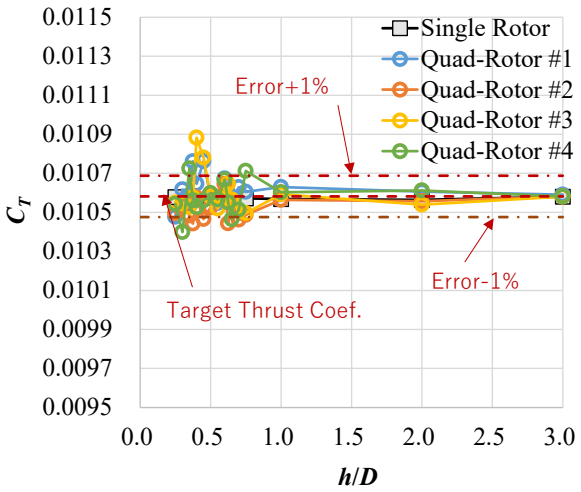

Figure 10. Thrust coefficient of each rotor after 60 revolutions

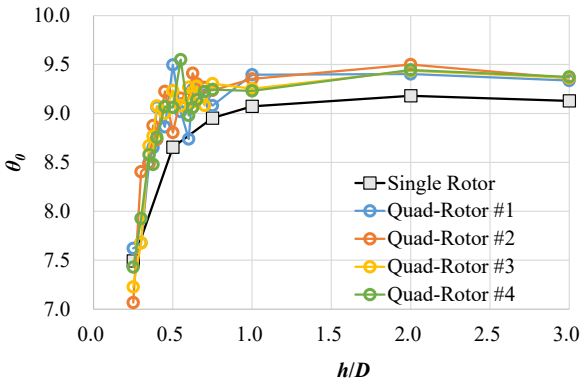

Figure 11. Pitch angles of each rotors

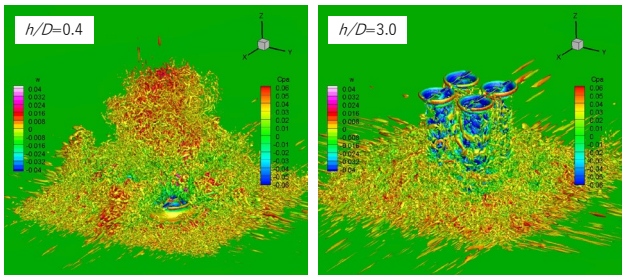

Figure 12. Flowfields around rotors for various rotor heights

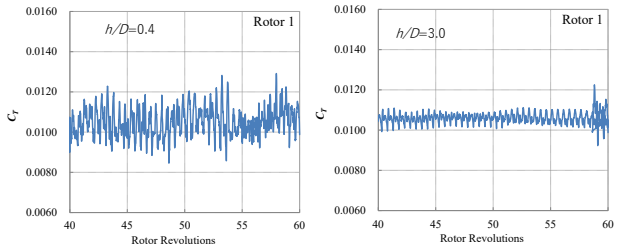

Figure 13. Thrust time histories for various rotor heights

4.3. Rotor performance in ground effect

Changes of the averaged required power per rotor are compared with the single rotor and the quadrotor drone where the central fuselage is included as shown in Fig. 14. The trends of the required powers are quite different from each other. As a result of interaction between the quad rotors, the required power for each of the quad rotors is about 3% higher than the single rotor OGE.

The ratios of the required power between IGE and OGE are compared in Fig. 15. The quadrotor drone shows the ground effect when the rotor height is below 2 rotor diameters. The ratio changes of the quad rotors and the single rotor are similar when the rotor height is greater than 0.75*D*. However, the quad rotors power change is not monotonically decreasing with the rotor height. The local increase of power indicates the occurrence of flow recirculation on the rotors. There is a large power increase at rotor height of 0.5*D* for the quadrotor drone. Detailed rotor flow trajectories showed the flow recirculation mainly occurred on the inner part of the rotors which is mainly influenced by the central fuselage. [5] The resolution of the rotor height for the quadrotor drone is coarser than the quadrotors. Similarly, finer rotor height change will be performed to determine the range of the rotor height that causes flow recirculation for the quadrotor drone.

The equivalent *Figures of Merit* (*FM*) as defined in Eq. (4) for the three configurations are shown in Fig. 16. The quad rotors without the central fuselage show the worst *FM* in the rotor height between 0.25*D* and 3.0*D*. Local up/down changes of the *FM* indicate the sensitivity of rotor performance with the rotor height.

The averaged rotor pitch angle changes with the rotor height are shown in Fig. 17. With the ground effect, the pitch angle for the single rotor monotonically decreases with the rotor height. For the quad rotors with/without the central fuselage, local increases of pitch angle are required to keep the same rotor thrust at some specific altitudes, which is one of the sources to cause instability of flight for the multirotor drones hovering near the ground.

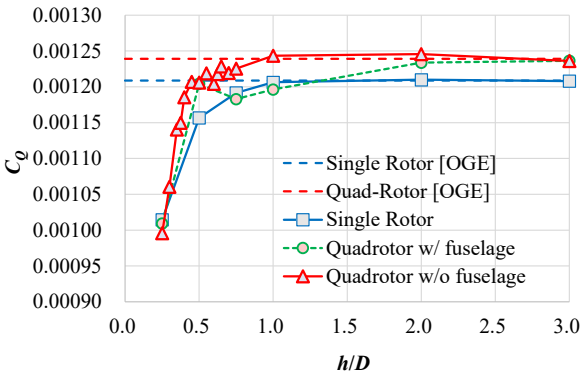

Figure 14. Required power for each rotor

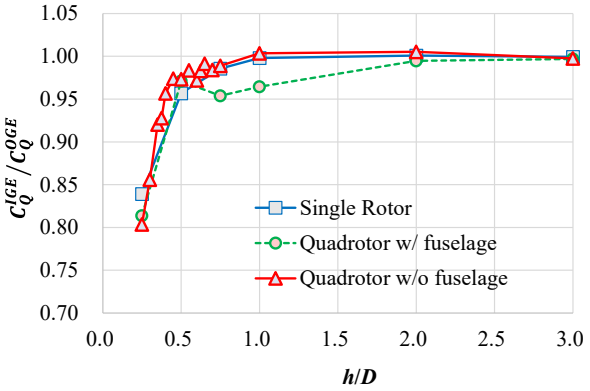

Figure 15. Required power ratios between IGE and OGE

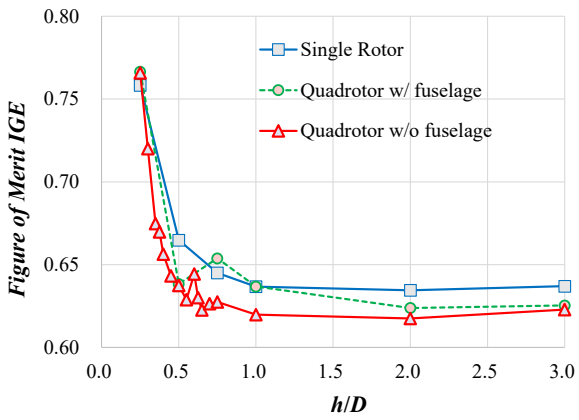

Figure 16. Rotor equivalent Figure of Merit IGE

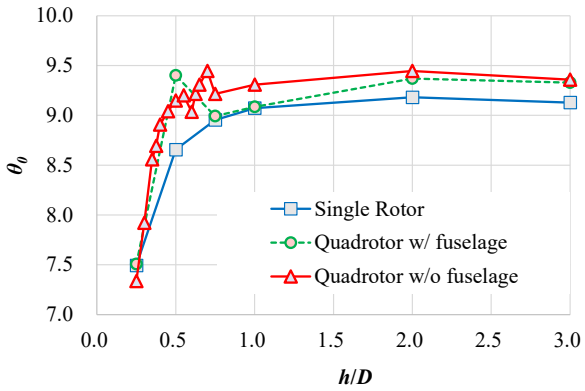

Figure 17. Averaged rotor pitch angle change IGE

4.4. Flowfields around quad rotors

The flowfields of the quad rotors at various rotor heights at 60 rotor revolutions from the start are shown in Fig. 18. The iso-surfaces of the Q-criterion are colored based on the velocity normalized by the sonic speed. The upwashes are observed mainly at the central portion of the rotors, and also along the gap between the rotors. The upwash increases with the decrease of the rotor height.

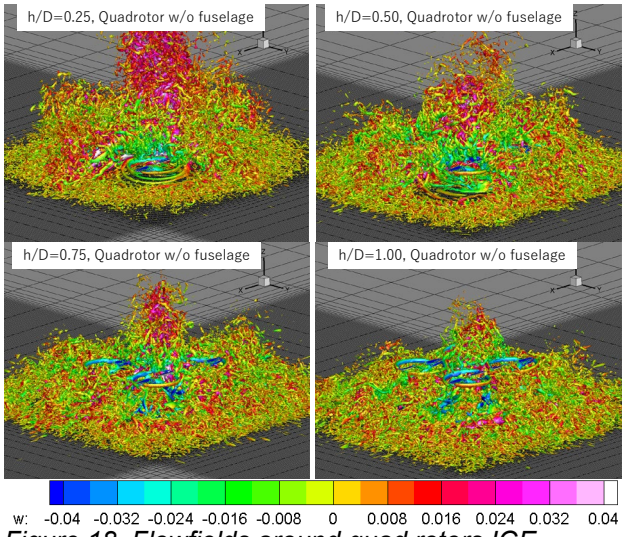

Figure 18. Flowfields around quad rotors IGE

Averaged flowfield is obtained by averaging the instantaneous flowfields from 57 to 60 rotor revolutions every 150 degrees of azimuth angle. The magnitude of velocity normalized by the rotor induced velocity on the section crossing the diagonal rotor centres and on the section along the gap between the rotors is shown the Fig. 19. The outwash on the section crossing the diagonal rotor centres looks likely to the single rotor, that the outwash flows along the ground. However, on the section along the rotor gap, the outwash exists also at the high altitude.

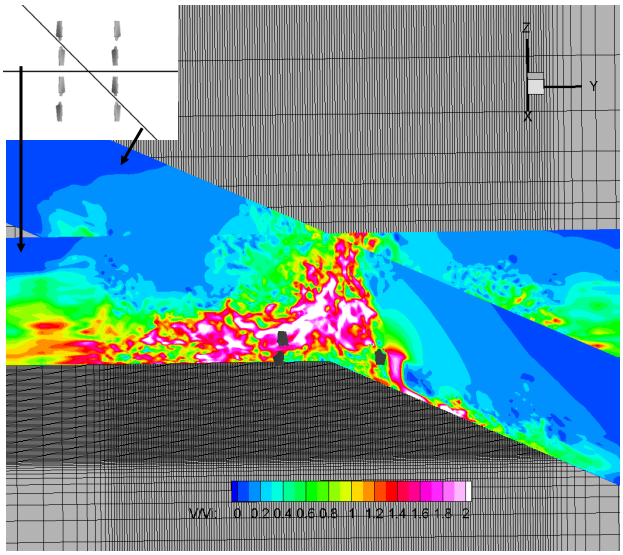

Figure 19. Averaged sectional flowfields for h/D=0.5

4.5. Outwash distributions

The flow speed averaged from 57 to 60 revolutions normalized by the rotor-induced velocity on the section is shown in Fig. 20. The quadrotor drone with the central fuselage is also shown for comparison. It is obvious that the upwash on the drone central portion is blocked by the central fuselage and redirected to the neighboring rotors. For the quad rotors without the central fuselage, downwash from the inner part of the rotor is reflected from the ground and forms a strong upwash. The upwash is not strictly symmetric, on this picture, interact heavily with the right rotor. It is corresponding to the larger rotor performance loss of this rotor. The unsteady nature of the flow around the rotors should be taken into account to realize stable flight controls.

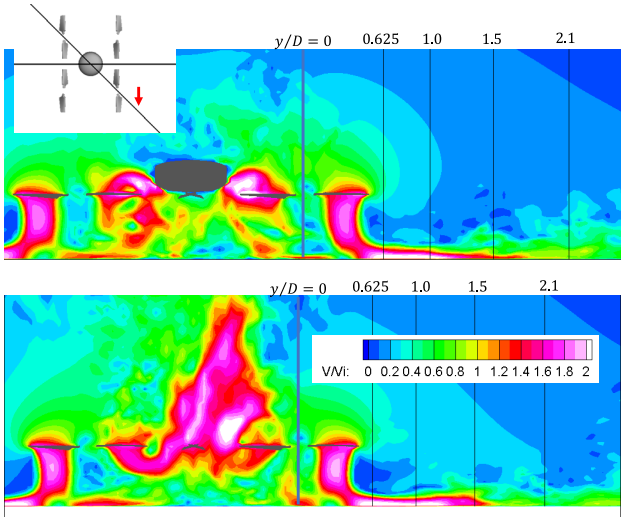

Figure 20. Velocity distributions on the section crossing the diagonal rotor centres

The averaged velocity profiles at stations *y/D*=0.625, 1.0, 1.5, and 2.1 are shown in Fig. 21. Please notice that *y/D*=0 is placed at the rotor center, not on the drone center. The velocity profiles for the three configurations look quite similar. At the near stations, *y/D*=0.65 and 1.0, outwash from the quad rotors is stronger and maximum velocity is near the ground. It can be concluded that on this section, the outwashes for the quad rotors and the quadrotor drone can be treated as same as the single rotor. It must be noted that this flow distribution may be significantly altered when the rotor distance gets nearer.

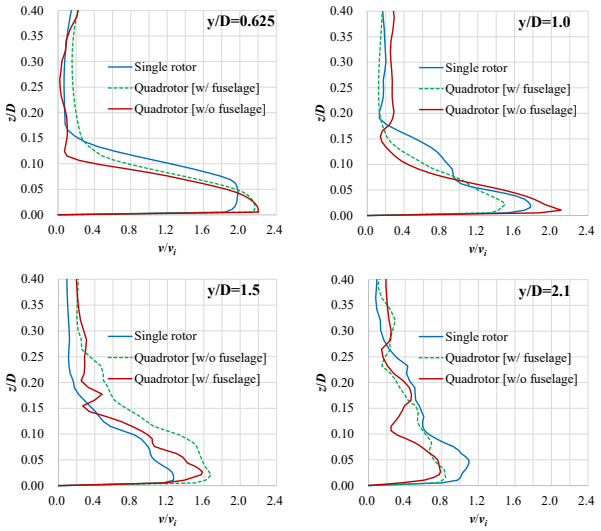

Figure 21. Comparisons of outwash velocity profiles on the section crossing the diagonal rotor centres

On the section along the gap of the rotors, as shown in Fig. 22, the outwash velocity distributions are compared between the quadrotor drone with the central fuselage and the quad rotors without the central fuselage. It can be observed that stronger outwash exists at higher altitude even at *y/D*=2.1 for the quadrotor drone.

The velocity profiles at several ground stations are shown in Fig. 23. Compared with the single rotor, the flow velocity near the ground is about the same. Comparing the quadrotor drone with the quad rotors without the central fuselage, strong outwash exists at higher altitude for both cases. Relatively, the outwash from the quadrotor drone with the central fuselage is stronger at all the stations.

Considering the operation of a quadrotor type eVTOL aircraft, the outwash distribution in the direction crossing the diagonal rotor centres is the same with a single rotor. The size (diameter) of a rotor in the quadrotor aircraft will be nearly half the size of a single-rotor helicopter to carry the same weight. That means the outwash will decay to a small velocity in about half of the distance. In the directions along the gap of the rotors, stronger outwash exists in higher altitude. This may cause some safety concern to the ground personnel nearby, although the stational maximum velocity in this direction will decay two times faster than a single rotor design.

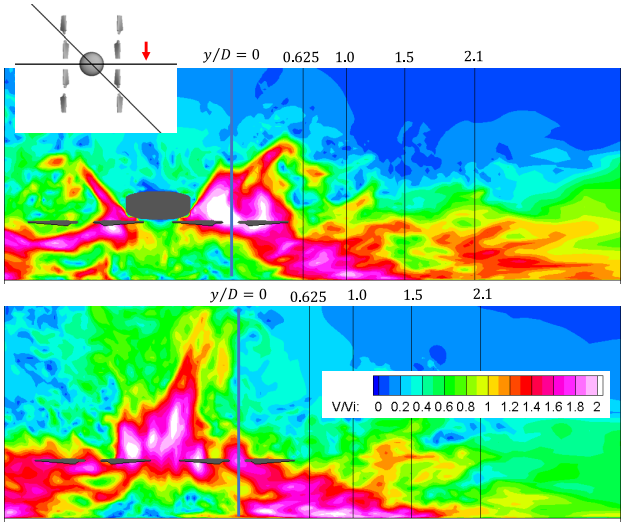

Figure 22. Velocity distribution on the section along the gap between the rotors

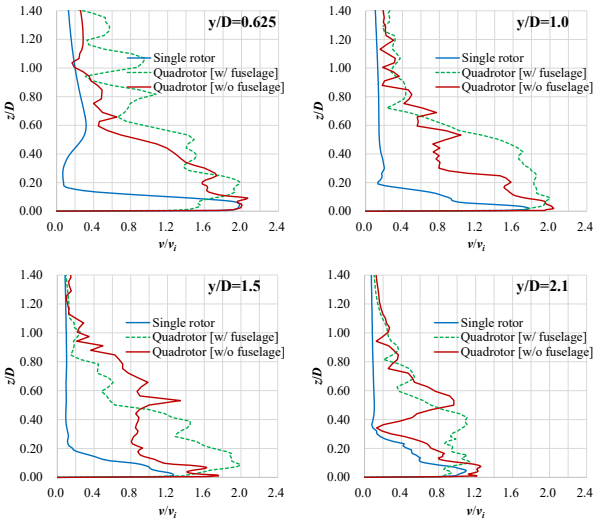

Figure 23. Comparisons of outwash velocity profiles on the section along the gap between the rotors

5. SUMMARY

Quad rotors in ground effect (IGE) are studied through high-fidelity numerical simulations:

Single rotor IGE results are validated with existing experimental data and excellent agreement is found for the required power changes and the outwash velocity profiles.

When the quadrotor height is within 0.25 to 0.75 rotor diameters, the flowfield is highly unsteady. The pitch angles may differ from each other to keep a constant

rotor thrust.

The required power change for the quad rotors with the rotor height is not monotonic as the single rotor case. Sensitive change of the required rotor power may cause difficulty of flight control during hovering flight at low altitudes.

Outwash from the quad rotors changes drastically with the direction of the quad rotors. On the sections crossing the diagonal rotor centres, the outwash profile resembles that of a single rotor. On sections along the gap of the rotors, outwash reaches a higher height, which may incur safety concerns for the ground personnel.

The central fuselage blocks the strong upwash in the centre of the drone. The flow recirculation around the rotor is obvious for this configuration at low rotor height about 0.5 rotor diameters.

As future works:

The influence of the rotor height on the outwash velocity will be examined.

The influence of the rotor distance to the ground effect is considered significant. The results will be published on following symposiums.

ACKNOWLEDGMENT

This study was financially supported by JSPS KAKENHI JP19H02344, as part of research on the "Enhancement of safety of manned and unmanned multi-rotor aircraft and assessment of influences to surroundings."

REFERENCES

[1] Kohno, M., Otsuka, H., Kiribayashi, S. and Nagatani, K., "Investigation on Relationship between Rotors Axis Length and Ground Effect on a Small Quadrotor UAV Performance," The Robotics and Mechatronics Conference 2017 in Fukushima, May 10-13, 2017. 1P2-F02. (in Japanese).

[2] Kohno, M., "Visualization of the Upstream Flow of Rotors and Analysis on Thrust of a Small Quadrotor UAV in Ground Effect," 55th Aircraft Symposium, Shimane, Japan, Nov. 20-22, 2017. JSASS-2017-5022. (in Japanese).

[3] Yonezawa, K. Matsumoto, H., Sugiyama, K., Tanabe, Y., Tokutake, H., and Sunada, S., "Aerodynamic Characteristics of a Quad-Rotor-Drone with Ducted Rotors," 8th Asian/Australian Rotorcraft Forum, Ankara, Turkey, Oct. 30-Nov. 2, 2019.

[4] Sunada, S., Tanabe, Y., Yonezawa, K., Tokutake, H., Umezaki, S., Yamaguchi, K. and Sugawara, H., "A study on Improvement of Performance of a Multiple Rotor Drone," Journal of the Robotics Society of Japan, Vol. 39, No. 4, pp. 357-362, 2021. (in Japanese).

[5] Tanabe, Y., Sugawara, H., Sunada, S., Yonezawa, K. and Tokutake, H., "Quadrotor Drone Hovering in Ground Effect," Journal of Robotics and Mechatronics, Vol.33, No.2, pp. 339-347, 2021.

[6] Tanabe, Y., Saito, S. and Sugawara, H., "Construction and Validation of an Analysis Tool Chain for Rotorcraft Active Noise Reduction," 38th European Rotorcraft Forum, Amsterdam, NL, Sept. 4-7, 2012.

[7] Tanabe, Y., Aoyama, T., Sugiura, M., Sugawara, H., Sunada, S., Yonezawa, K. and Tokutake, H., "Multiple Rotors Hovering Near an Upper or a Side Wall," Journal of Robotics and Mechatronics, Vol. 30, No. 3, pp. 344-353, 2018.

[8] Tanabe, Y., Aoyama, T., Sugiura, M., Sugawara, H., Sunada, S., Yonezawa, K. and Tokutake, H., "Numerical Simulations of Aerodynamic Interactions Between Multiple Rotors," 42nd ERF, Lille, France, Sept. 6-9, 2016.

[9] Shima, E., and Kitamura, K., "On New Simple Low-Dissipation Scheme of AUSM-Family for All Speeds," 47th AIAA Aerospace Sciences Meeting, Orlando, FA, January 5-8, 2009, AIAA Paper 2009-136.

[10] Tanabe, Y. and Saito, S., "Significance of All-Speed Scheme in Application to Rotorcraft CFD Simulations," The 3rd International Basic Research Conference on Rotorcraft Technology, Nanjing, China. October 14-16, 2009.

[11] Yamamoto, S. & Daiguji, H., "Higher-Order-Accurate Upwind Schemes for Solving the Compressible Euler and Navier-Stokes Equations," Computers & Fluids, Vol.22, No.2/3, pp.259-270, 1993.

[12] Zhang, L.P. & Wang, Z.J., "A Block LU-SGS Implicit Dual Time-Stepping Algorithm for Hybrid Dynamic Meshes," Computers & Fluids, Vol.33, pp.891–916, 2004.

[13] Jameson, A. and Baker, T. J., "Solution of the Euler equations for Complex Configuration," Proceedings of 6th Computational Fluid Dynamics Conference Danvers, AIAA Paper 83-1929, Danvers, MA, USA, July 1983. https://doi.org/ 10.2514/6.1983-1929

[14] Tanabe, Y., Sugawara, H., Yonezawa, K., Sunada, S. and Tokutake, H., "Influence of Rotor Blade Twist on Ducted Rotor Performance," 8th Asian/Australian Rotorcraft Forum, Ankara, Turkey, Oct. 30 – Nov. 2, 2019.

[15] Schmaus, J., Berry, B., Gross, W., and Koliais, P., "Experimental Study of Rotor Performance in Deep Ground Effect with Application to a Human-Powered Helicopter," American Helicopter Society 68th Annual Forum, Fort Worth, TX, May 2012.

[16] O'Bryan, T., "An Investigation of the effect of downwash from a VTOL aircraft and a helicopter in the ground environment," NASA TN D-977, 1961.
[17] Usuda H., Iboshi N. and Itoga N., "Ground effect of a hovering rotor over confined area," 45th Aircraft Symposium, Kitakyushu, Japan, October 10-12, 2007. (In Japanese).
[18] Tanabe, Y., Saito, S., Ooyama, N. and Hiraoka, K., "Study of a Downwash Caused by a Hovering Rotor in Ground Effect," 34th European Rotorcraft Forum, Liverpool, UK, Sept. 16-19, 2008.

Presented at 47th European Rotorcraft Forum, United Kingdom, 7-9th September, 2021